ACS APPLIED MATERIALS & INTERFACES

Research Article

www.acsami.org

From GaN to $ZnGa_2O_4$ through a Low-Temperature Process: Nanotube and Heterostructure Arrays

Ming-Yen Lu,[†,*,‡] Xiang Zhou,[†] Cheng-Yao Chiu,[‡] Samuel Crawford,[†] and Silvija Gradečak*[,†]

[†]Department of Materials Science and Engineering, Massachusetts Institute of Technology, Cambridge, Massachusetts 02139, United States

[‡]Graduate Institute of Opto-Mechatronics, National Chung Cheng University, Chia-Yi 62102, Taiwan

Supporting Information

ABSTRACT: We demonstrate a method to synthesize GaN−$ZnGa_2O_4$ core−shell nanowire and $ZnGa_2O_4$ nanotube arrays by a low-temperature hydrothermal process using GaN nanowires as templates. Transmission electron microscopy and X-ray photoelectron spectroscopy results show that a $ZnGa_2O_4$ shell forms on the surface of GaN nanowires and that the shell thickness is controlled by the time of the hydrothermal process and thus the concentration of Zn ions in the solution. Furthermore, $ZnGa_2O_4$ nanotube arrays were obtained by depleting the GaN core from GaN−$ZnGa_2O_4$ core−shell nanowire arrays during the reaction and subsequent etching with HCl. The GaN−$ZnGa_2O_4$ core−shell nanowires exhibit photoluminescence peaks centered at 2.60 and 2.90 eV attributed to the $ZnGa_2O_4$ shell, as well as peaks centered at 3.35 and 3.50 eV corresponding to the GaN core. We also demonstrate the synthesis of GaN−$ZnGa_2O_4$ heterojunction nanowires by a selective formation process as a simple route toward development of heterojunction nanodevices for optoelectronic applications.

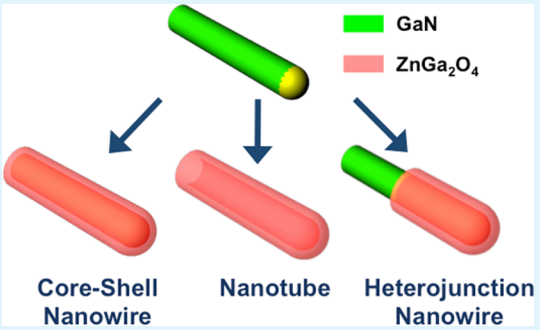

KEYWORDS: *gallium nitride (GaN), zinc gallate ($ZnGa_2O_4$), heterostructures, nanotubes, hydrothermal method, optical property*

1. INTRODUCTION

Heterojunction nanowires and nanotubes with different geometries − including radial,[1,2] axial,[3−5] and branched structures[6,7] − offer superior properties compared to their uniform-composition counterparts and broaden potential applications including field effect transistors,[8] light emitting diodes,[9,10] lasers,[11] and energy harvesting devices.[12] Among different nanostructured materials, significant effort has been made to synthesize $ZnGa_2O_4$, a spinel material with a wide band gap of 4.4−4.7 eV. $ZnGa_2O_4$ has attracted much attention in recent years owing to its potential applications in diverse areas, including light emitting diodes,[13] photodetectors,[14] and photocatalysts,[15] or as a transparent conducting oxide,[16] especially for applications that require transparency from violet to near ultraviolet wavelengths. When doped with Mn^{2+} and Cr^{3+} as activation centers, emission of $ZnGa_2O_4$ can be tuned from blue to red and therefore it can also be used as a low-voltage multicolor-emitting phosphor.[17] Moreover, $ZnGa_2O_4$ has been reported to be a stable photoanode in photoelectrochemical water splitting when combined with ZnO to form heterostructures.[18]

However, except for limited reports on hydrothermal synthesis of $ZnGa_2O_4$ nanoparticles at low temperatures,[19−24] most synthesis routes for such one-dimensional spinel nanostructures require high-temperature processes. Li et al. and Chang et al. synthesized $ZnGa_2O_4$ nanotube arrays at temperatures around 1000 °C using ZnO and Ga_2O_3 nanowire arrays as templates, respectively.[25,26] Xu and coworkers fabricated single-crystalline $ZnGa_2O_4$ nanowire by thermal evaporation using mixture of ZnO, Ga_2O_3, and graphite powders.[27] Forming nanowire heterostructures using these methods is also challenging, as this process requires precise control over the growth parameters (e.g. temperature, pressure, and sources). A low-temperature liquid-phase process would provide a simple, controllable, and lower cost alternative to synthesize $ZnGa_2O_4$ nanomaterials and heterostructures. Herein, we report the formation of well-aligned GaN−$ZnGa_2O_4$ core−shell (CS) nanowire, $ZnGa_2O_4$ nanotube, and GaN−$ZnGa_2O_4$ heterojunction arrays via a low-temperature hydrothermal process. The crystal structures and optical properties of these nanostructures are discussed. The low-temperature selective formation of GaN-$ZnGa_2O_4$ heterojunction nanostructures is also demonstrated.

2. EXPERIMENTAL DETAILS

GaN nanowire arrays were synthesized using a hot-wall horizontal-flow metal organic chemical vapor deposition (MOCVD) system on *r*-plane sapphire substrates via the vapor-liquid-solid (VLS) growth mechanism, as previously described.[28,29] The substrates were first cleaned by sonication in acetone, methanol, and deionized water before depositing 1 nm and 5 nm thick gold seed films by electron beam evaporation. Ammonia (50 sccm) and nitrogen (400 sccm) were

Received: September 23, 2013
Accepted: December 19, 2013
Published: December 19, 2013

 © 2013 American Chemical Society

injected through the background line, whereas tri-methyl gallium (13 °C, 500 Torr, 0.85 sccm H_2) was supplied from a separate injector line using hydrogen (150 sccm) as the carrier gas. The growth chamber was heated to 850°C in nitrogen, and hydrogen was briefly supplied before the introduction of the III and V sources to reduce any oxides on the metal films. The growth was carried out at 100 Torr and 850 °C for 80 min. As-obtained GaN nanowire arrays were then used as templates to fabricate GaN−$ZnGa_2O_4$ CS nanowire arrays and $ZnGa_2O_4$ nanotube arrays. Uniform GaN−$ZnGa_2O_4$ core−shell nanowire arrays were prepared using an aqueous solution of zinc nitrate hexahydrate [$Zn(NO_3)_2{\cdot}6H_2O$] and hexamethylenetetramine [$C_6H_{12}N_4$, HMTA] with equal concentrations ranging from 0.1 to 1 mM. GaN nanowire templates were placed upside down in the solution and the sealed solution was heated to 85 °C for 1.5−8 h. $ZnGa_2O_4$ nanotube arrays were obtained by selective etching of the GaN core using 5% HCl(aq) for 15−30 min.

The morphology, chemical composition, and structure of as-prepared nanostructures were characterized by field-emission scanning electron microscopy (FESEM, JEOL JSM-6320 FV), X-ray photoelectron spectrectroscopy (XPS, Ulvac-PHI PHI 1600), and scanning transmission electron microscopy (STEM, JEOL JEM-2010F). STEM equipped with an energy-dispersive X-ray spectrometer (EDS) was used to analyze the chemical composition of the nanostructures. Fast Fourier filtering of the high-resolution TEM images was applied using Digital Micrograph software to improve the signal to noise ratio. The optical properties of GaN−$ZnGa_2O_4$ CS nanowires on *r*-sapphire substrates were studied by a home-built photoluminescence (PL) system using a 262 nm excitation laser with an effective pumping power density of 800 Wcm^{-2}.

3. RESULTS AND DISCUSSION

Due to the epitaxial relationships between GaN and *r*-plane sapphire substrates, MOCVD-grown GaN nanowires used in this work grow along the non-polar *m*-direction and form an angle of approximately 60° with the substrate, in agreement with the previous study.[28] First, GaN−$ZnGa_2O_4$ CS nanowire arrays were obtained by hydrothermal reaction on a GaN nanowire array template in 0.5 mM zinc nitrate and HMTA equimolar solution at 85 °C for 3 h. The resulting core−shell nanowires preserve the epitaxial relationship with the substrate, as revealed using SEM (Figure 1a). The low magnification TEM image of a single GaN-$ZnGa_2O_4$ CS nanowire in Figure 1b shows a distinct change in contrast along the radial direction of the nanowire, indicating the formation of a core−shell structure. The corresponding selected area diffraction (SAD) in Figure 1c shows two distinct patterns: a spot pattern corresponding to the single-crystalline wurtzite GaN core and a ring pattern indicating a polycrystalline spinel $ZnGa_2O_4$ shell (the complete diffraction pattern is provided in Figure S1a in the Supporting Information). Finally, elemental profiles obtained from EDS linescans across individual GaN−$ZnGa_2O_4$ core-shell nanowires (Figure 1d) show that zinc and oxygen are present in the shell only, whereas gallium is detected across the entire nanowire diameter. The shape of Ga line profile and the plateau in the middle of nanowire of Zn and O profiles is consistent with the triangular cross-section of *m*-directional GaN nanowire templates with $ZnGa_2O_4$ shell. Taken together, these results confirm that our process transforms surface of the GaN nanowire to form a $ZnGa_2O_4$ shell, resulting in a GaN−$ZnGa_2O_4$ core−shell structure.

Starting from the core−shell structure, $ZnGa_2O_4$ nanotubes can be obtained by immersing the core-shell nanowires in HCl. HCl penetrates through the grain boundaries in the polycrystalline $ZnGa_2O_4$ to reach the core and selectively etch away GaN, resulting in a tubelike structure. The dark-field STEM image of a single $ZnGa_2O_4$ nanotube in Figure 2a clearly shows the

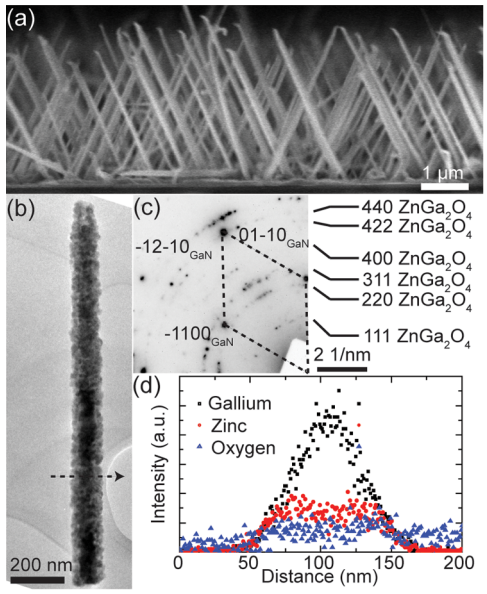

Figure 1. (a) SEM image of GaN−$ZnGa_2O_4$ CS nanowire arrays. (b) TEM image of a representative GaN-$ZnGa_2O_4$ CS nanowire and (c) the corresponding selected area diffraction pattern taken along the [0002] zone axis of GaN confirms the presence of GaN and $ZnGa_2O_4$. (d) EDS linescan profiles of Ga, Zn, and O acquired across the CS nanowire along the arrow shown in b.

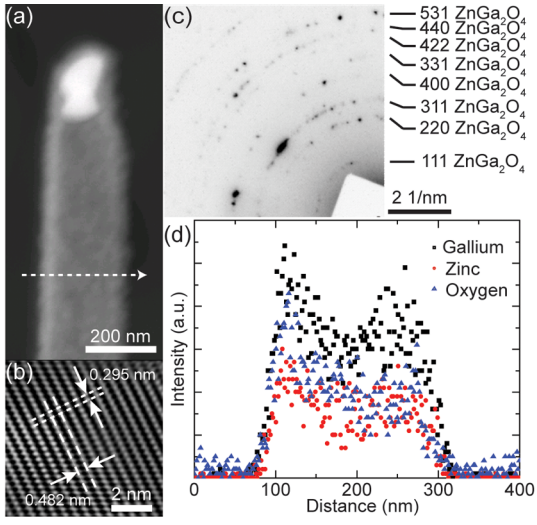

Figure 2. (a) Dark-field STEM image of a single $ZnGa_2O_4$ nanotube. The bright contrast at the tip is due to the gold catalyst used to grow GaN nanowires. (b) Atomic resolution TEM image from the $ZnGa_2O_4$ shell depicting *d*-spacing of 0.295 and 0.482 nm correspond to (−220) and (111) of $ZnGa_2O_4$, respectively. The image has been Fourier filtered using Digital Micrograph. (c) Corresponding selected area diffraction pattern of the nanotube, where all diffraction rings can be assigned to $ZnGa_2O_4$. (d) EDS linescan profiles of $ZnGa_2O_4$ nanotube along the arrow shown in a, confirming that the shell is composed of Ga, Zn, and O.

tubular contrast (the bright contrast at the top of nanotube is a gold nanoparticle used to grow the GaN nanowire). Furthermore, the high-resolution TEM image of the $ZnGa_2O_4$ nanotube (Figure 2b) shows atomic spacings of 0.482 nm and 0.295 nm corresponding to (111) and (220) planes of $ZnGa_2O_4$, respectively. The SAD pattern of nanotube in Figure 2c also confirms that the nanotube is composed of

dx.doi.org/10.1021/am404158f | ACS Appl. Mater. Interfaces 2014, 6, 882−887

polycrystalline $ZnGa_2O_4$ whereas the wurtzite GaN core is completely etched out, as confirmed by the absence of GaN diffraction spots as observed in Figure 1c (the complete diffraction pattern is provided in Figure S1b in the Supporting Information). Also, no reflections corresponding to ZnO and Ga_2O_3 are found in the diffraction pattern (see Figure S2 in the Supporting Information). Finally, the EDS linescan profiles of Ga, Zn, and O across the nanotube diameter (Figure 2d) show the decrease in Ga, Zn, and O signal in the center of the nanotube, confirming the tubular geometry.

The chemical states and composition of the samples were further investigated using XPS. Figure 3a shows the survey scan

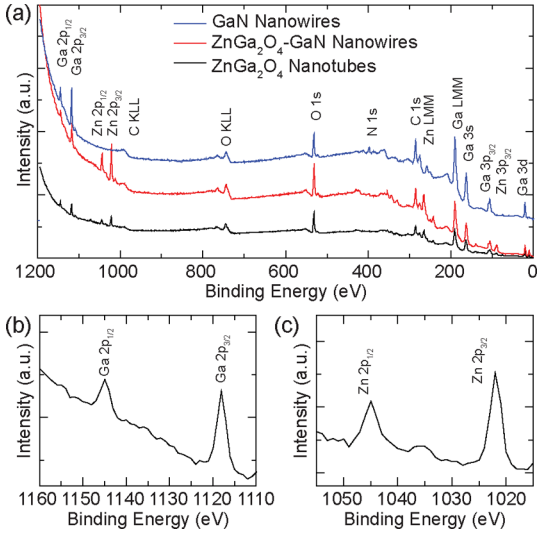

Figure 3. (a) XPS survey scan of GaN nanowires, GaN–$ZnGa_2O_4$ CS nanowires and $ZnGa_2O_4$ nanotubes. (b, c) XPS spectra of Ga 2p and Zn 2p for $ZnGa_2O_4$ nanotubes. The energy separation (ΔE) between Ga $2p_{3/2}$ and Zn $2p_{3/2}$ peaks is 96 eV, which indicates complete formation of spinel $ZnGa_2O_4$ shell.

with the binding energy ranging from 0 to 1200 eV for GaN nanowires, GaN–$ZnGa_2O_4$ CS nanowires, and $ZnGa_2O_4$ nanotubes. The compositional evolution can be recognized in the spectra: Zn peaks emerged after the hydrothermal reaction, whereas the N signal diminished after the hydrothermal reaction and then disappeared after the etching process, indicating the formation of GaN–$ZnGa_2O_4$ CS nanowires and $ZnGa_2O_4$ nanotubes, respectively. Furthermore, the detailed XPS spectra of Ga and Zn signals are depicted in panels b and c in Figure 3, respectively. In this work, for the $ZnGa_2O_4$ nanotubes obtained by the low-temperature hydrothermal process, the ΔE between Ga $2p_{3/2}$ and Zn $2p_{3/2}$ peaks is 96 eV, consistent with the results from $ZnGa_2O_4$ powders prepared by a high temperature solid-state reaction.[30] Moreover, the XPS spectra of N 1s from GaN NWs and GaN-$ZnGa_2O_4$ CS NWs in Figure S3 in the Supporting Information show the binding energies (397.5 eV) are almost the same, which implies that the chemical state of nitrogen remains unchanged.

The reaction time of the hydrothermal reaction was varied in order to understand the structural transformation of the GaN–$ZnGa_2O_4$ core–shell nanowires. Figure 4a–d shows TEM images of the GaN–$ZnGa_2O_4$ core–shell nanowires synthesized with processing times ranging from 1.5 to 8 h. The shell thickness increases rapidly at the early stage of the reaction, but

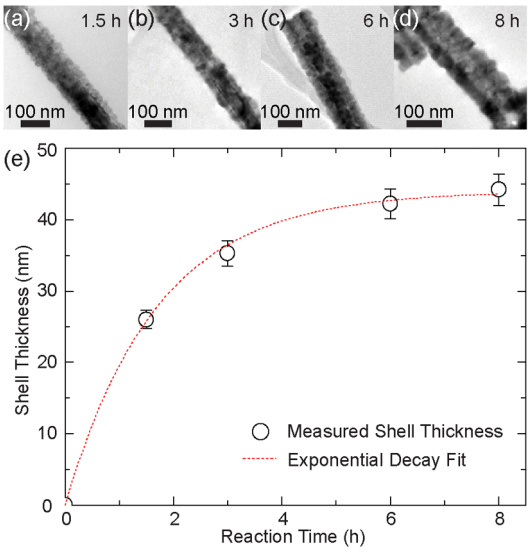

Figure 4. (a–d) TEM images of GaN–$ZnGa_2O_4$ CS nanowires grown in 0.5 mM zinc nitrate and HMTA equimolar solution at 85 °C for 1.5, 3, 6, and 8 h, respectively. (e) Thickness of $ZnGa_2O_4$ shells as a function of the reaction time. The red dashed curve shows the exponential fit to the experimental results according to eq 1.

then slows down and saturates (Figure 4e). It is worthwhile to note that the presence of GaN core is always observed, even for hydrothermal reactions up to 1 day (data not shown), during which Zn ions from the solution are mostly consumed. This result implies that the formation rate of $ZnGa_2O_4$ shell is strongly dependent upon the availability of Zn ions in the solution.[31] In principle, GaN can be fully transformed to $ZnGa_2O_4$ by supplying the fresh reaction solution of zinc nitrate and HMTA. However, to control the shell thickness, forming a partial core–shell structure followed by HCl etching of the core is preferred. Assuming that the reaction rate to form $ZnGa_2O_4$ is directly proportional to the zinc ion concentration in the solution, and that the rates of any competing reactions that deplete zinc ions (e.g., ZnO precipitation) are also proportional to the concentration, we can deduce the following equation relating $ZnGa_2O_4$ shell thickness to reaction time (see the Supporting Information for more details)

$$R = C_2(1 - e^{-rt}) \quad (1)$$

Here, R is the shell thickness, C_2 is a geometric constant, r is the rate constant for the depletion of Zn^{2+} ions, and t is reaction time. Figure 4e shows the experimentally measured shell thickness as a function of the reaction time and the excellent fit based on this growth model.

The formation of $ZnGa_2O_4$ in this work is attributed to the presence of HMTA, which decomposes to formaldehyde and ammonia in aqueous solution. Ammonia further forms ammonium hydroxide during the reaction.[32]

$$C_6H_{12}N_4 + 6H_2O \rightarrow 6CH_2O + 4NH_3 \quad (2)$$

$$NH_3 + H_2O \rightarrow NH_4^+ + OH^- \quad (3)$$

The OH^- species, formed during the hydrolysis of ammonia, play an important role in forming the metal ion complex in two aspects. First, $Zn(OH)_3^-$ is formed from the reaction of Zn^{2+} in the solution with OH^-. Second, GaN nanowires can be wet-etched in a basic medium and form Ga_2O_3, which can be further dissolved to form $Ga(OH)_4^-$. Eventually, $Zn(OH)_3^-$

dx.doi.org/10.1021/am404158f | ACS Appl. Mater. Interfaces 2014, 6, 882–887

and $Ga(OH)_4^-$ react in the solution to precipitate $ZnGa_2O_4$.[33,34] The dominant chemical reactions discussed above can be described as follows

$$Zn^{2+} + 3OH^- \rightarrow Zn(OH)_3^- \quad (4)$$

$$2GaN + 3H_2O \rightarrow Ga_2O_3 + 2NH_3 \text{ (in the presence of } OH^-) \quad (5)$$

$$Ga_2O_3 + 3H_2O \rightarrow 2Ga(OH)_3 \quad (6)$$

$$Ga(OH)_3 + OH^- \rightarrow Ga(OH)_4^- \quad (7)$$

$$Zn(OH)_3^- + 2Ga(OH)_4^- \rightarrow ZnGa_2O_4 + 4H_2O + 3OH^- \quad (8)$$

A recent theoretical study showed the formation enthalpy of $ZnGa_2O_4$ from ZnO and Ga_2O_3 is −0.90 eV, which confirms that $ZnGa_2O_4$ is thermodynamically more stable than its respective oxides.[35] Noticeably, we observed that by increasing the temperature from 75 to 90 °C, the shell formation rate is higher. However, to model the growth rate, we considered only the reaction at 85 °C, as the amount of Zn in the solution is the most important parameter for the reaction to form $ZnGa_2O_4$.

Heterostructures with spatially modulated composition may possess unique optical properties due to the combination of emission from both the core and shell. The PL spectra of GaN-$ZnGa_2O_4$ CS nanowires, $ZnGa_2O_4$ nanotubes and, for reference, a blank *r*-sapphire substrate are summarized in Figure 5. The PL spectrum of GaN−$ZnGa_2O_4$ CS nanowires

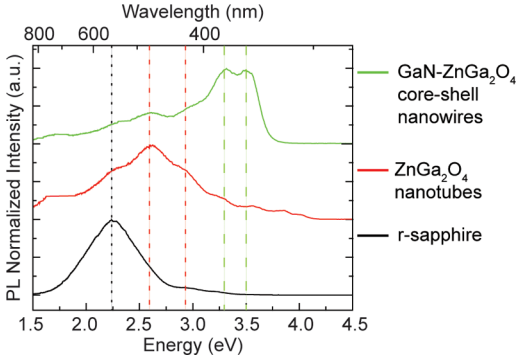

Figure 5. Normalized PL spectra of GaN−$ZnGa_2O_4$ CS nanowires, $ZnGa_2O_4$ nanotubes, and *r*-sapphire. Black dotted line indicates emission from *r*-sapphire substrate, red dotted lines indicate position of PL emission from $ZnGa_2O_4$ (2.6 and 2.9 eV), and green dotted lines indicate emission from GaN (3.35 and 3.5 eV). Some emission from GaN could still be observed from $ZnGa_2O_4$, because of a small amount of GaN residue after HCl etching.

shows peaks associated with GaN centered at 3.35 and 3.5 eV. The 3.35 eV peak is associated with donor-bound emission, and the blue-shifted bandgap luminescence at 3.5 eV peak from GaN can be attributed to a compressive strain and/or Al diffusion from the sapphire substrate.[29] In addition, we also observed peaks around 2.6 and 2.9 eV, which have been observed in $ZnGa_2O_4$ nanoparticles,[36] and are therefore attributed to the $ZnGa_2O_4$ shell. These two peaks become dominant in the PL spectra of $ZnGa_2O_4$ nanotubes, whereas the GaN peaks almost completely disappear. The shoulder in the spectrum centered around 2.25 eV can be ascribed to the underlying *r*-sapphire substrate. Overall, the PL spectra confirmed the presence of GaN and $ZnGa_2O_4$ in the nanowires and the absence of GaN in the $ZnGa_2O_4$ nanotubes. These results also indicated that the $ZnGa_2O_4$ shell formed at the expense of GaN nanowires during the hydrothermal reaction.

To fabricate devices for advanced applications, heterojunctions are often needed; however, heterostructures are typically fabricated at high temperature using expensive growth equipment. Here, we demonstrate that our low-temperature approach can be used to synthesize heterojunction nanowires. Figure 6 schematically describes the selective formation procedures of GaN-$ZnGa_2O_4$ heterostructures. GaN nanowire arrays epitaxially grown on *r*-sapphire were first filled with polymethyl methacrylate (PMMA, MicroChem, 495 PMMA A5) by spin-coating. The PMMA layer was then etched using O_2 plasma until the GaN nanowires emerged about 1 μm from the PMMA surface. The substrates were then immersed into the solution for reaction with the exposed GaN nanowire sections, and the residual PMMA layer was removed by acetone after the end of the reaction. Because the PMMA layer serves as a blocking layer for the formation of $ZnGa_2O_4$ shells, the length of $ZnGa_2O_4$ shells on GaN nanowires therefore can be controlled by the etching parameters of the PMMA layer.

Images a and b in Figure 7 show SEM and low-magnification TEM images of a single GaN-$ZnGa_2O_4$ heterojunction nanowire, respectively. The SEM image reveals that the upper part of the nanowire has rough surface and thicker diameter than that of the lower part of the nanowire, implying the shell formation on the GaN nanowire. The low-magnification TEM image shows that the thick upper segment of the nanowire has a radial variation in contrast, indicating the presence of a polycrystalline shell composed of columnar-shaped particles with sizes ranging from 40 to 60 nm (see Figure S4 in the Supporting Information). The diffraction pattern from the CS nanowire is shown in Figure 7c : in addition to a pattern of dots from the single-crystalline GaN nanowire, the rings in the diffraction pattern correspond to spinel $ZnGa_2O_4$ (the complete diffraction pattern is provided in Figure S1c in the Supporting Information). The high- resolution TEM images obtained from surfaces in the upper and lower portions of the heterostructure in Figure 7b are shown in images d and e in Figure 7, respectively. The 0.485 nm lattice fringe in Figure 7d agrees with the (111) plane of $ZnGa_2O_4$, and the 0.279 nm and 0.52 nm spacings correspond to the (−1100) and (0001) planes of GaN, respectively. Overall, our results confirm selective formation of the nanowire shell enabled by PMMA masking.

Our low-temperature selective core-shell formation strategy may be adopted to develop p−n junction nanostructures for optoelectric nanodevices when p-GaN is used as the core. $ZnGa_2O_4$ can be doped to emit multicolor light in the visible region; thus, GaN−$ZnGa_2O_4$ CS nanowires with modulated doping could potentially be used for the development of electrically driven white-light emitters when incorporated with a GaN nanowire as the core. Furthermore, the $ZnGa_2O_4$ shell may be an effective surface passivation layer for the GaN core because of the higher band gap of $ZnGa_2O_4$.

4. CONCLUSIONS

GaN−$ZnGa_2O_4$ CS nanowire arrays have been synthesized via a hydrothermal process using the GaN nanowire arrays as templates and as a source of Ga in the reaction. After obtaining GaN−$ZnGa_2O_4$ CS nanowires, spinel $ZnGa_2O_4$ nanotube arrays were obtained by depleting the GaN core during the

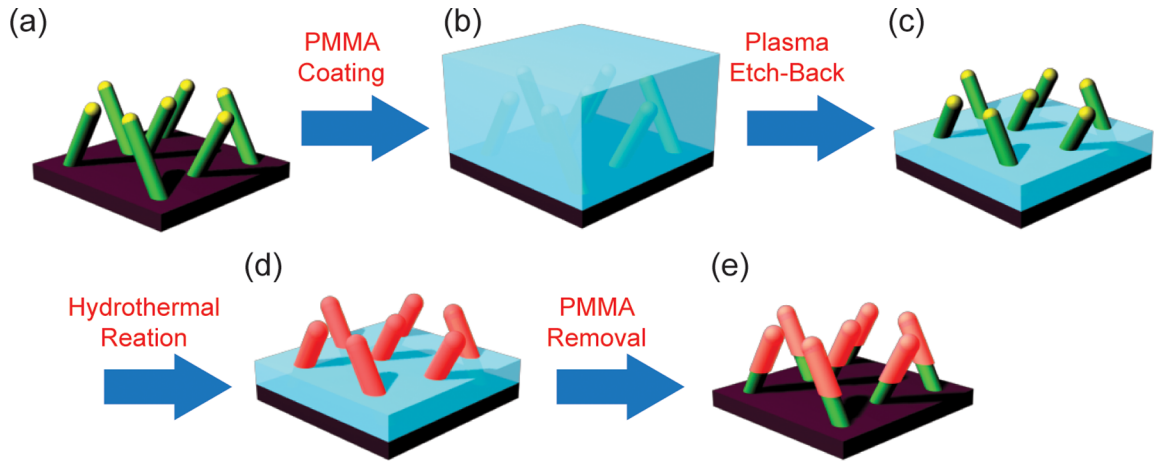

Figure 6. Schematic illustration of the selective shell formation procedure. (a) GaN nanowire arrays were grown using MOCVD and then used as templates to synthesize heterostructures. (b) PMMA was spun over the GaN nanowire array substrates, and (c) GaN nanowires were partially exposed after oxygen plasma etching. (d) $ZnGa_2O_4$ shells were grown by the low temperature hydrothermal method, and (e) GaN-$ZnGa_2O_4$ CS heterojunction nanowire arrays remained after PMMA removal.

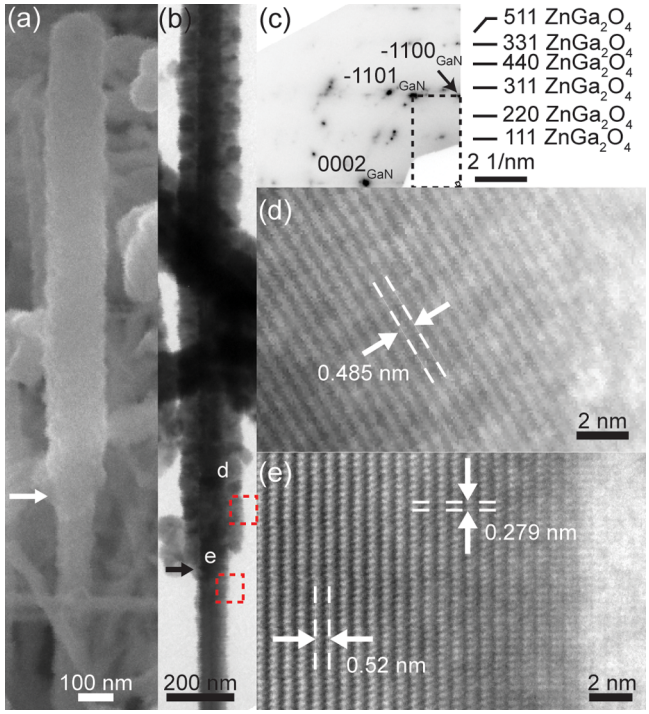

Figure 7. (a) SEM image of a single GaN−$ZnGa_2O_4$ CS heterojunction nanowire. (b) Low-magnification TEM image and (c) the corresponding selected area diffraction pattern of a single GaN−$ZnGa_2O_4$ CS heterojunction nanowire. The diffraction pattern reveals a periodic spot pattern of the GaN core and ring patterns of the $ZnGa_2O_4$ shell. Fourier-filtered atomic resolution TEM images from the marked regions in b, revealing the lattice fringes of (d) $ZnGa_2O_4$ and (e) GaN.

reaction and further etching it in HCl solution. TEM results confirmed the formation of GaN−$ZnGa_2O_4$ CS nanowires, and EDS mapping and XPS data confirmed the compositions of spinel $ZnGa_2O_4$ shell. Although the thickness of the $ZnGa_2O_4$ shell increased with the reaction time, the final shell thickness is limited by the total amount of Zn ions in the solution. The $ZnGa_2O_4$ shell thickness could be further controlled by the initial concentration of Zn ion in the reaction solution. The structural results were confirmed by photoluminescence spectra from GaN−$ZnGa_2O_4$ CS nanowires, which exhibit multiple peaks originating from from both the $ZnGa_2O_4$ shell and the GaN core. We also demonstrated the capability of a low-temperature selective formation process to synthesize the GaN−$ZnGa_2O_4$ heterojunction nanostructures, which can be a promising method to fabricate heterojunction nanostructures for advanced applications such as photodetectors, and energy harvesting devices. Moreover, the $ZnGa_2O_4$ shell has the potential to become a convenient phosphor to convert part of the GaN-emitted UV light to green and red, thus enabling white-light-emitting diodes.

■ ASSOCIATED CONTENT

Ⓢ Supporting Information

Full scale selected area electron diffraction patterns, XPS spectra of GaN NWs and GaN-$ZnGa_2O_4$ CS NWs, and calculations of the $ZnGa_2O_4$ formation rate. This material is available free of charge via the Internet at http://pubs.acs.org.

■ AUTHOR INFORMATION

Corresponding Authors

*E-mail: mylu@ccu.edu.tw.
*E-mail: gradecak@mit.edu.

Notes

The authors declare no competing financial interest.

■ ACKNOWLEDGMENTS

This work was supported by the Center for Excitonics, an Energy Frontier Research Center funded by the US Department of Energy, Office of Basic Energy Sciences under Award Number DE-SC0001088, and the National Science Council (NSC) in Taiwan (NSC 101-2218-E-194-002 and NSC 102-2221-E-194-055). The authors acknowledge the use of the MRSEC Shared Experimental Facilities at MIT, supported by the National Science Foundation under Award DMR-08-19762.

■ REFERENCES

(1) Lauhon, L. J.; Gudiksen, M. S.; Wang, C. L.; Lieber, C. M. *Nature* **2002**, *420*, 57−61.
(2) Qian, F.; Li, Y.; Gradecak, S.; Wang, D. L.; Barrelet, C. J.; Lieber, C. M. *Nano Lett.* **2004**, *4*, 1975−1979.

(3) Gudiksen, M. S.; Lauhon, L. J.; Wang, J.; Smith, D. C.; Lieber, C. M. *Nature* **2002**, *415*, 617−620.
(4) Lu, M. Y.; Song, J. H.; Lu, M. P.; Lee, C. Y.; Chen, L. J.; Wang, Z. L. *ACS Nano* **2009**, *3*, 357−362.
(5) Lim, S. K.; Crawford, S.; Haberfehlner, G.; Gradecak, S. *Nano Lett.* **2013**, *13*, 331−336.
(6) Lu, M. Y.; Su, P. Y.; Chueh, Y. L.; Chen, L. J.; Chou, L. J. *Appl. Surf. Sci.* **2005**, *244*, 96−100.
(7) Wang, D.; Qian, F.; Yang, C.; Zhong, Z. H.; Lieber, C. M. *Nano Lett.* **2004**, *4*, 871−874.
(8) Lieber, C. M.; Li, Y.; Xiang, J.; Qian, F.; Gradecak, S.; Wu, Y.; Yan, H.; Yan, H.; Blom, D. A. *Nano Lett.* **2006**, *6*, 1468−1473.
(9) Qian, F.; Gradecak, S.; Li, Y.; Wen, C. Y.; Lieber, C. M. *Nano Lett.* **2005**, *5*, 2287−2291.
(10) Zhang, X. M.; Lu, M. Y.; Zhang, Y.; Chen, L. J.; Wang, Z. L. *Adv. Mater.* **2009**, *21*, 2767−2770.
(11) Qian, F.; Li, Y.; Gradecak, S.; Park, H. G.; Dong, Y. J.; Ding, Y.; Wang, Z. L.; Lieber, C. M. *Nat. Mater.* **2008**, *7*, 701−706.
(12) Lieber, C. M.; Tian, B. Z.; Zheng, X. L.; Kempa, T. J.; Fang, Y.; Yu, N. F.; Yu, G. H.; Huang, J. L. *Nature* **2007**, *449*, 885−U888.
(13) Yu, C. F.; Lin, P. *J. Mater. Sci. Lett.* **1998**, *17*, 555−557.
(14) Lee, Y. E.; Norton, D. P.; Budai, J. D.; Wei, Y. *J. Appl. Phys.* **2001**, *90*, 3863−3866.
(15) Zhang, W. W.; Zhang, J. Y.; Chen, Z. Y.; Wang, T. M. *Catal. Commun.* **2009**, *10*, 1781−1785.
(16) Omata, T.; Ueda, N.; Ueda, K.; Kawazoe, H. *Appl. Phys. Lett.* **1994**, *64*, 1077−1078.
(17) Gu, Z. J.; Liu, F.; Li, X. F.; Howe, J.; Xu, J.; Zhao, Y. L.; Pan, Z. W. *J. Phys. Chem. Lett.* **2010**, *1*, 354−357.
(18) Zhong, M.; Li, Y. B.; Yamada, I.; Delaunay, J. J. *Nanoscale* **2012**, *4*, 1509−1514.
(19) Hirano, M.; Sakaida, N. *J. Am. Ceram. Soc.* **2002**, *85*, 1145−1150.
(20) Li, Y.; Duan, X.; Liao, H.; Qian, Y. *Chem. Mater.* **1998**, *10*, 17−18.
(21) Hirano, M. *J Mater Chem* **2000**, *10*, 469−472.
(22) Vasile, M.; Vlazan, P.; Avram, N. M. *J. Alloys Compd.* **2010**, *500*, 185−189.
(23) Yuan, Y.; Du, W.; Qian, X. *J. Mater. Chem.* **2012**, *22*, 653−659.
(24) Yan, S.; Wang, J.; Gao, H.; Wang, N.; Yu, H.; Li, Z.; Zhou, Y.; Zou, Z. *Adv. Funct. Mater.* **2013**, *23*, 758−763.
(25) Li, Y. J.; Lu, M. Y.; Wang, C. W.; Li, K. M.; Chen, L. J. *Appl. Phys. Lett.* **2006**, 88,.
(26) Chang, K. W.; Wu, J. J. *J. Phys. Chem. B* **2005**, *109*, 13572−13577.
(27) Xu, L.; Su, Y.; Zhou, Q. T.; Li, S.; Chen, Y. Q.; Feng, Y. *Cryst. Growth Des.* **2007**, *7*, 810−814.
(28) Lim, S. K.; Crawford, S.; Gradecak, S. *Nanotechnology* **2010**, *21*, 345604.
(29) Zhou, X.; Chesin, J.; Crawford, S.; Gradecak, S. *Nanotechnology* **2012**, *23*, 285603.
(30) Zou, L.; Xiang, X.; Wei, M.; Li, F.; Evans, D. G. *Inorg. Chem.* **2008**, *47*, 1361−1369.
(31) Ashfold, M. N. R.; Doherty, R. P.; Ndifor-Angwafor, N. G.; Riley, D. J.; Sun, Y. *Thin Solid Films* **2007**, *515*, 8679−8683.
(32) Weintraub, B.; Deng, Y. L.; Wang, Z. L. *J. Phys. Chem. C* **2007**, *111*, 10162−10165.
(33) Zhuang, D.; Edgar, J. H. *Mater. Sci. Eng., R* **2005**, *48*, 1−46.
(34) Chen, L. M.; Liu, Y. N.; Lu, Z. G.; Huang, K. L. *Mater. Chem. Phys.* **2006**, *97*, 247−251.
(35) Dixit, H.; Tandon, N.; Cottenier, S.; Saniz, R.; Lamoen, D.; Partoens, B.; Speybroeck, V. V.; Waroquier, M. *New J. Phys.* **2011**, *13*, 063002.
(36) Dutta, D. P.; Ghildiyal, R.; Tyagi, A. K. *J. Phys. Chem. C* **2009**, *113*, 16954−16961.